DOI: 10.1002/chem.201000593

On the Mechanism of Ruthenium-Catalyzed Formation of Hydrogen from Alcohols: A DFT Study

Adam Johannes Johansson, Erik Zuidema, and Carsten Bolm*[a]

Abstract: The mechanism of the ruthenium-catalyzed dehydrogenation of methanol has been investigated by using three DFT-based methods. Three pathways were considered in which the ruthenium catalyst was ligated by either two or three phosphine ligands. Dispersion interactions, which are not described by the popular B3LYP functional, were taken into account by using the dispersion-corrected B3LYP-D and M06 density functionals. These interactions were found to be important in the description of reaction steps that involved ligand/substrate/product association with or dissociation from the catalyst. In line with experimental results, the resting state of the catalyst was predicted to be a ruthenium trihydride complex. It is shown that the dehydrogenation reaction preferentially proceeds through pathways in which the catalyst is ligated by two phosphine ligands. The catalytic cycle of the dehydrogenation process involves an intermolecular proton transfer from the methanol substrate to the catalyst followed by the release of dihydrogen. Rate-determining β-hydride elimination from the resulting methoxide species then regenerates the resting state of the catalyst and completes the catalytic cycle. The overall free-energy barriers of 29.6–31.4 kcal mol^{-1} predicted by the three density functionals are in good agreement with the experimentally observed reaction rate of 6 h^{-1} at 423 K.

Keywords: dehydrogenation · dispersion interactions · hydrogen · reaction mechanisms · ruthenium

Introduction

Owing to the dwindling amounts of fossil fuel resources and the ever-growing energy demand of the world, a large number of alternative, more sustainable energy sources are being explored more intensively than ever. Among these, hydrogen is a highly attractive and clean source of energy (as long as storage problems can be overcome) as well as an important component of many proposed production routes for transportation fuels and other chemicals from renewable resources.[1] The current industrial production of hydrogen through the steam-reforming of methane is not sustainable and so alternatives need to be developed. The cleanest and most sustainable process would be the catalytic splitting of water, but despite tremendous progress in the development of such a process over the last few years,[2] its large-scale application is still far from being realized. As an alternative, lignocellulosic biomass is a potential renewable source of hydrogen,[3] but the production of hydrogen from biomass through steam-reforming has proven less straightforward than the steam-reforming of methane.[4]

On the other hand, chemical and enzymatic depolymerization processes coupled with other (bio)chemical transformations can convert the main components of biomass into a wide variety of small molecules in a relatively energy-efficient way.[5] These molecules always contain one or more alcohol moieties, which can be oxidized to useful aldehydes, ketones, or carboxylic acids. When these oxidation reactions are performed in the absence of a hydrogen-accepting oxidant, this leads to the formation of hydrogen as a byproduct. These processes are often referred to as dehydrogenation or acceptorless oxidation processes.[6] Based on the existing knowledge of the steam-reforming of hydrocarbons, heterogeneous catalysts and processes using these catalysts have been developed that efficiently produce hydrogen from re-

[a] Dr. A. J. Johansson, Dr. E. Zuidema, Prof. Dr. C. Bolm
Institute of Organic Chemistry, RWTH Aachen University
Landoltweg 1, 52056 Aachen (Germany)
Fax: (+49) 241-809-2391
E-mail: Carsten.Bolm@oc.rwth-aachen.de

Supporting information for this article is available on the WWW under http://dx.doi.org/10.1002/chem.201000593. Free-energy diagrams for base-independent pathways for the $P(CH_3)_3$ model, free-energy diagram for the full system determined by using the density functional M06, Cartesian coordinates for all optimized minima and transition states, and the computed free energies for methoxide–methanol solvation complexes.

newable resources, albeit still with significant byproduct formation and still needing high reaction temperatures (500 °C).[7]

Homogeneous catalysts, which normally operate at much lower temperatures and generally have higher chemoselectivities than heterogeneous catalysts, are comparatively underdeveloped for these dehydrogenation processes. Nevertheless, the first example of a catalytic dehydrogenation of alcohols using homogenous catalysts was reported as early as 1975.[8] Over the years, several catalysts based on different metals have been explored in this reaction,[9] but they did not lead to large increases in the efficiency of hydrogen production. In the late eighties, Morton and Cole-Hamilton and co-workers obtained promising results using the dehydrogenation catalyst $[RuN_2H_2(PPh_3)_3]$ at a relatively low reaction temperature of 150 °C.[10] Unlike many other studies on homogeneous catalysts for hydrogen production, a variety of primary and secondary alcohols were successfully dehydrogenated with turnover frequencies (TOF) of 6–524 h^{-1}. A mechanism was proposed (Scheme 1) in which the dinitrogen ligand of the catalyst precursor is initially displaced by an alkoxide moiety that is generated from the alcoholic substrate under the basic conditions used (1 M NaOH). The resulting alkoxide complex can then undergo hydride transfer from the alkoxide to the metal to form the aldehyde or ketone product and the anionic ruthenium trihydride complex $[RuH_3(PPh_3)_3]^-$. This trihydride complex was suggested to be the resting state of the catalyst under the reaction conditions. It was proposed that this complex is protonated by the alcohol substrate[11] to yield the neutral ruthenium tetrahydride complex $[RuH_4(PPh_3)_3]$ and generate a new alkoxide species. To complete the catalytic cycle, dihydrogen is released and the dihydride complex $[RuH_2(PPh_3)_3]$ is formed in a reductive-elimination-type reaction. It was argued that for this catalyst, the release of dihydrogen is rate limiting and that the three PPh_3 ligands remain coordinated to the metal center during the process. Later studies, however, revealed that additional phosphine in the reaction mixture retards the reaction,[12] which indicates that the reaction mechanism probably involves ligand dissociation. These studies also suggested that not hydrogen release but β-hydride elimination of the ruthenium-alkoxy species is the rate-determining step in the catalytic cycle.

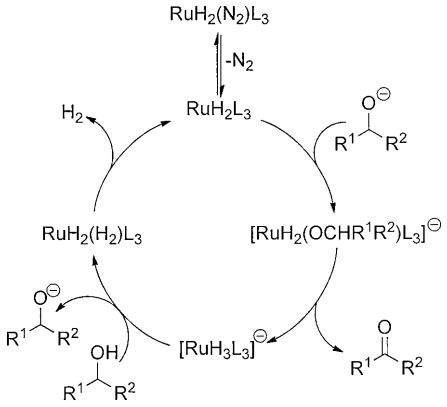

Scheme 1. Proposed catalytic cycle for the dehydrogenation of alcohols catalyzed by $[RuN_2H_2(PPh_3)_3]$.

Because experimental support for the proposed mechanism and the resting state of the catalyst is still rather limited, further rational development of more active and stable catalysts is hampered. Beller and co-workers increased the activity of the system by exchanging the PPh_3 ligands for more bulky and electron-donating phosphine ligands[13] or more readily available and more stable amine ligands.[14] This suggests that electron-donating ligands enhance the reaction rate (in sharp contrast to earlier results[12]), but how they do this has remained unclear. Note also that several authors have recently reported interesting catalyst systems in which the ligand actively participates in the dehydrogenation process by temporarily "storing" one of the hydrogen atoms abstracted from the alcohol.[15] Clearly the operational modes of these catalysts differ from Cole-Hamilton's and Beller's catalysts for which the reaction occurs exclusively at the metal center. So, although these new catalysts provide valuable alternatives to metal-centered catalysts, they do not contribute to a better understanding of the original catalyst system.

To gain more insight into the reaction mechanism of the dehydrogenation of alcohols by ruthenium we have undertaken a systematic computational study of the dehydrogenation of methanol to formaldehyde catalyzed by the archetypal ruthenium–triphenylphosphine catalyst system. The mechanism proposed by Morton and Cole-Hamilton (Scheme 1) has been considered as one of several possible reaction pathways. Base-dependent as well as base-independent pathways have been investigated to explain the experimental need for basic reaction conditions (1 M NaOH).[10] Also, the effect of dissociation of one of the spectator ligands on the reaction has been explored. To understand the effects caused by noncovalent interactions (dispersion forces), results obtained by the classical B3LYP density functional method were compared with those obtained with the dispersion-corrected functionals B3LYP-D and M06.

Computational Methods and Models

The geometries were optimized in gas phase using the hybrid density functional B3LYP[16] and the LACVP basis set as implemented in Jaguar 7.0.[17] LACVP is the split valence Pople-style basis set 6-31G, supplemented by the Los Alamos effective core potential for ruthenium.[18] The geometries were optimized until the changes in the energy were less than 5×10^{-5} Hartrees (0.03 kcal mol^{-1}), and until the average change in the force (gradient) was smaller than 3×10^{-4} Hartrees $Bohr^{-1}$. Final gas phase electronic energies were evaluated using the larger polarized triple zeta basis set LACV3P** (6-311G(d,p) plus the Los Alamos ECP for ruthenium) and the B3LYP[16] and M06[19] functionals in Jaguar 7.0,[17] and the B3LYP-D[20] functional in Turbomole 6.0.[21] In the B3LYP-D calculations, the default dispersion coefficients and global scaling factor developed for B3LYP were used.

Hessian matrices composed of harmonic force constants were computed using Gaussian 03.[22] The Hessians were used for transition state optimizations and for the calculation of vibrational contributions to the thermodynamic potentials *H* (enthalpy) and *S* (entropy).[23] All transition states were verified to be first order saddle points on the potential energy surface by having one imaginary frequency in the Hessian of the optimized structure.

Basis set super position errors (BSSE) on bond-dissociation energies (BDE) calculated using LACV3P** were evaluated using the Counter–Poise scheme[24] and Jaguar 7.0.[17] This was only performed for the dissociation of the PPh_3 ligand from the catalyst, in light of large BSSE that were recently reported by Sieffert and Bühl for similar systems.[25] The BSSE for LACV3P** is found to be approximately 5 kcal mol^{-1} for the dissociation of one PPh_3 ligand from a ruthenium complex containing a total of three PPh_3 ligands. This BSSE is only about 50% of the error reported by Bühl, but it is unusually large for DFT calculations using large polarized triple zeta basis sets.

Long-range dielectric solvent effects on the relative energies of gas phase optimized structures were evaluated using the SCRF model and the Poisson–Boltzmann solver in Jaguar 7.0.[26] The solvent methanol was defined by a dielectric constant (ε) of 33.6 and a probe radius of 2.0 Å. In selected cases, the geometries of a model complex containing $P(Me)_3$ ligands (up to 46 atoms) were optimized in solution (SCRF), but this resulted in only minor changes in the final energies. It has been shown that gas phase geometries obtained at the B3LYP/DZ level are generally sufficiently accurate for the determination of reaction mechanisms.[27]

Many of the pathways explored below involve one or more reaction steps in which a proton is transferred from the methanol solvent to the catalyst. In these steps, a methoxide anion (CH_3O^-) is created. It reacts with the catalyst in a subsequent step. In order to approximate the energetics of these steps, the relative stability of this small anionic species under experimentally applied reaction conditions needs to be evaluated. To mimic the stabilizing effect of solvation of this species as realistically as possible, the free energies of its solvation by up to four hydrogen-bonded methanol molecules was evaluated (see page SI-1 in the Supporting Information).[28]

The geometries of these flexible and anionic complexes were optimized in solution (SCRF). At the high temperature at which the dehydrogenation reaction is performed (T = 423 K), which is above the boiling point of methanol, the only complex that is stable with respect to the free methoxy anion consists of the methoxide anion and a single methanol molecule. Even this complex is close in energy to the free anion (ΔG = 0.5 kcal mol^{-1}). The fact that larger aggregates are less stable can be attributed to the large entropy penalties associated with aggregation at high temperature, and to the stabilization of anionic species by dielectric effects (taken into account by the SCRF model).

Note that the absolute dielectric stabilization of these negatively charged species, predicted by the implicit solvation model, are very large (see page SI-1 in the Supporting Information). The effect is inversely dependent on the cavity size, and so stabilizes small anions such as the methoxide anion with respect to larger ones. As a consequence, the computed free energies of reaction steps that involve methoxide coordination to the catalyst include large positive solvent effects of around 20 kcal mol^{-1} (depending on the model) and should be regarded as approximate.

Results and Discussion

Reaction pathways: Initially, different dehydrogenation pathways were investigated by using a simplified model complex in which the PPh_3 ligands were substituted by $P(CH_3)_3$ ligands. For this model, all possible conformations and all intermediates and transition states were fully optimized. The most stable conformation was chosen for each intermediate to construct the free-energy diagrams. Note that for most intermediates and transition states there were two or more conformations very similar in energy (less than 2 kcal mol^{-1}). The pathways found to have the lowest activation energies in the $P(CH_3)_3$ model were subsequently reinvestigated by using the full catalyst (including the PPh_3 ligands). As a starting point of our investigations, the ruthenium complex $[Ru(MeO)H_2(PR_3)_3]^-$ (in which R is a methyl group in the model or a phenyl group in the full system) was chosen. This complex is generated from the catalyst precursor $[RuN_2H_2(PR_3)_3]$ by replacement of the labile N_2 ligand by a methoxide ion under the reaction conditions used. Starting from this complex, three possible pathways for hydrogen generation were systematically explored (Scheme 2).

In pathway **A**, one of the phosphine ligands in the complex $[Ru(MeO)H_2(PR_3)_3]^-$ (**1**) decoordinates to generate pentacoordinated species $[Ru(MeO)H_2(PR_3)_2]^-$ (**2**). All of the subsequent steps in this reaction pathway then proceed through complexes that contain only two phosphine ligands. From the coordinatively unsaturated methoxide complex **2**, β-hydride transfer from the coordinated methoxide ion to ruthenium can take place to yield formaldehyde complex **3**. In the second part of this pathway, the formaldehyde is exchanged for a new methanol molecule in a dissociative process and the O–H bond of this species is cleaved heterolytically. The proton forms a dihydrogen moiety with one of the hydrides of the complex and the methoxide ion remains coordinated to ruthenium. Displacement of the dihydrogen ligand then yields methoxide complex **2** again, completing the catalytic cycle. Alternatively, trihydride complex **4** can be protonated by the methanol solvent without the resulting methoxide coordinating to the metal (it instead being solvated). Release of hydrogen then generates the highly unsaturated intermediate **8** to which a methoxide can coordinate. This is designated as pathway **B**.

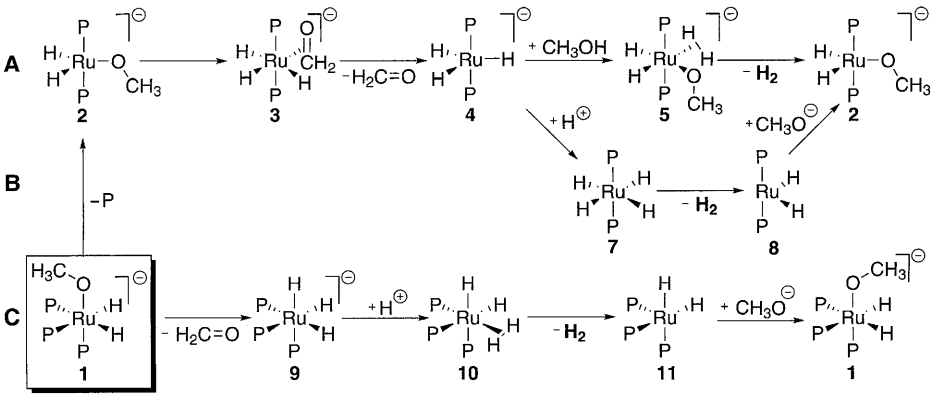

Scheme 2. Dehydrogenation pathways considered in this study. P represents the $P(CH_3)_3$ or PPh_3 ligands.

In pathway **C**, the reaction proceeds without phosphine dissociation. β-Hydride transfer from the coordinated methoxide ion to the ruthenium in complex **1** then occurs through a heptacoordinated transition state to yield the trihydride complex $[RuH_3(PR_3)_3]^-$ (**9**). As in pathway **B**, one of the hydride ligands of this complex can be protonated by the solvent followed by release of dihydrogen and coordination of a new methoxide moiety to reform the starting complex **1**.

We also explored two base-independent pathways. Under neutral conditions the concentration of methoxide anions in solution is vanishingly small. Therefore the N_2 ligand of the catalyst precursor $[RuN_2H_2(PR_3)_3]$ will be replaced by a neutral methanol molecule instead of a methoxide moiety under these conditions. We found, however, that these pathways did not compete with the base-dependent pathways described above. This was in line with the experimental need for a base (1 M NaOH).[10] The free-energy diagrams for these pathways will therefore not be presented here but are given in the Supporting Information.

The $P(CH_3)_3$-ligated model: The calculated free energies of the pathways for the simplified model are shown in Figure 1. For both pathways **A** and **B**, the initial dissociation of $P(CH_3)_3$ from $\mathbf{1_S}$ is highly exergonic ($\Delta G<0$) by -13 kcal mol^{-1} and results in the formation of the bipyramidal complex $[RuH_2(CH_3O^-)\{P(CH_3)_3\}_2]^-$ ($\mathbf{2_S}$). We attribute the large energy gain of this dissociation step to the unfavorable *trans* arrangement of the CH_3O^- ion and one of the hydride ligands in reactant $\mathbf{2_S}$. When the phosphine ligand is removed, the complex rearranges without an enthalpy barrier to a trigonal-bipyramidal structure in which the methoxide is no longer directly *trans* to any of the hydrides. If we compare this step to the dissociation of a phosphine ligand from $[RuH_3\{P(CH_3)_3\}_3]$ ($\mathbf{9_S}$; see below) in which there is no hydride–methoxide *trans* effect ($\Delta G=-0.6$ kcal mol^{-1}), this reorganization contributes to a large part of the exergonicity of the phosphine dissociation from $\mathbf{1_S}$.

From species $\mathbf{2_S}$ there is a modest free-energy barrier of 10.1 kcal mol^{-1} for β-hydride transfer from the methoxide ligand to ruthenium (the optimized transition state $\mathbf{TS_{S2,3}}$ is shown in Figure 2). This step yields $[Ru(CH_2{=}O)H_3P(Me_3)_2]^-$ ($\mathbf{3_S}$) in which the formaldehyde molecule is only weakly coordinated to the metal. In pathway **A**, the formaldehyde moiety dissociates ($\Delta G=3.5$ kcal mol^{-1}) to yield the square-pyramidal complex $[RuH_3\{P(CH_3)_3\}_2]^-$ ($\mathbf{4_S}$). Coordination of methanol to this complex is endergonic by 10 kcal mol^{-1} and the hypothetical intermediate $[Ru(CH_3OH)H_3\{P(CH_3)_3\}_2]^-$ should therefore not be regarded as a stable intermediate but rather a state on the way to the transition state for intramolecular proton transfer from the incoming methanol molecule to the ruthenium complex $\mathbf{4_S}$.

Although $\mathbf{4_S}$ is most stable when the two phosphine moieties adopt a mutual *cis* arrangement (Figure 2), the lowest

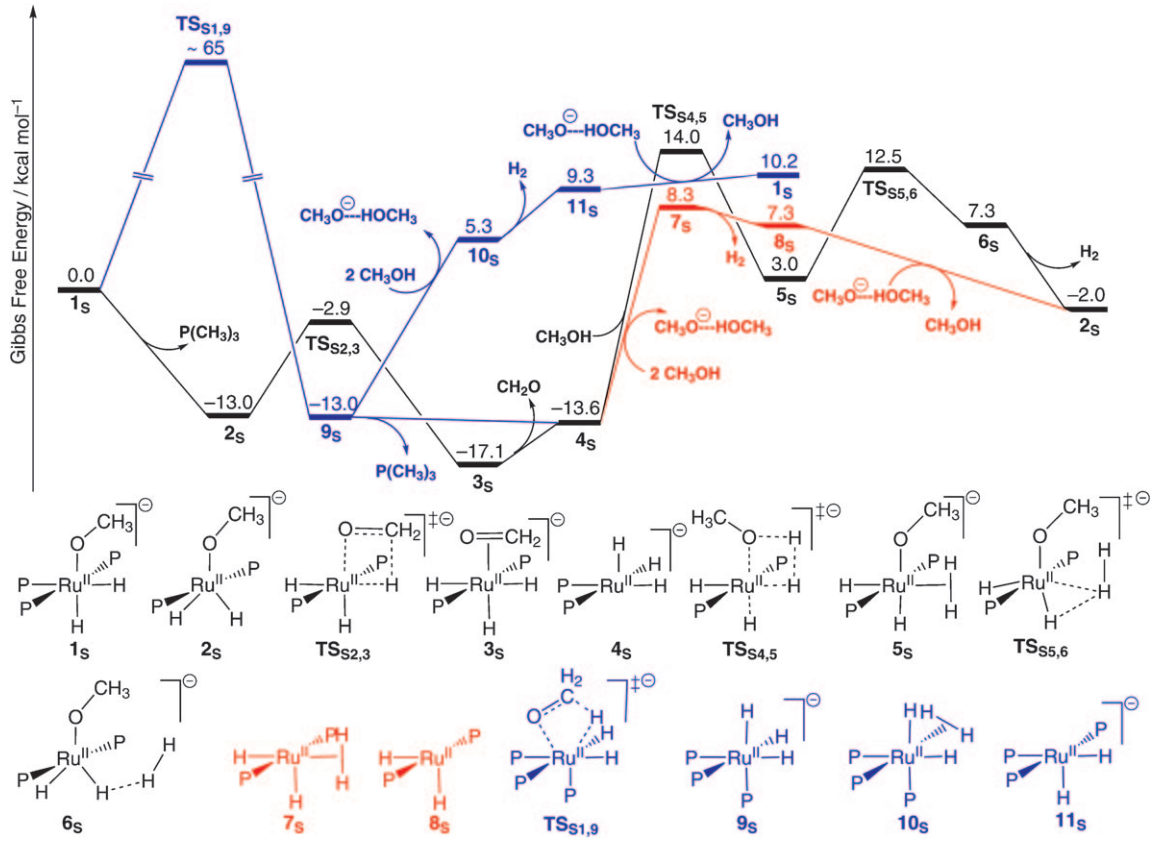

Figure 1. Free-energy profiles for base-dependent pathways **A**, **B** and **C** for the $P(CH_3)_3$-ligated system. P represents the $P(CH_3)_3$ ligand.

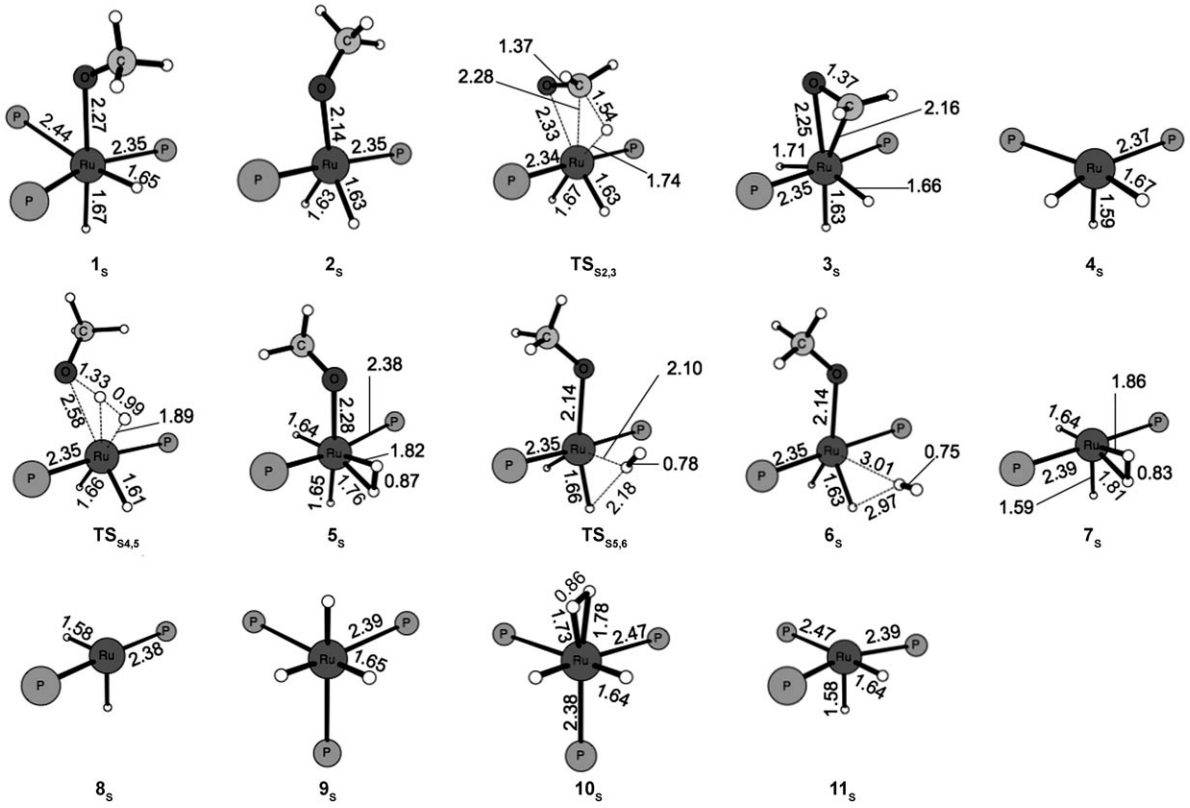

Figure 2. Structures of intermediates and transition states in pathways **A**, **B**, and **C** for the $P(CH_3)_3$-ligated model. The methyl groups of the $P(CH_3)_3$ ligands have been omitted for clarity. Distances are given in Ångströms.

barrier for proton transfer was found for an isomer in which the two phosphine ligands are coordinated *trans* to one another and therefore a conformational change must occur in $\mathbf{4_S}$ before the transition state $\mathbf{TS_{S4,5}}$. The barrier for this concerted proton transfer and coordination of the methoxide moiety is considerable ($\Delta G = 27.6\ \mathrm{kcal\,mol^{-1}}$) and the resulting dihydride–dihydrogen complex $[RuH_2(H_2)(CH_3O)\{P(CH_3)_3\}_2]^-$ ($\mathbf{5_S}$) is 16.6 kcal mol^{-1} higher in energy than reactant $\mathbf{4_S}$. The direct release of dihydrogen from this high-energy intermediate was considered, but instead a transition state was found for a process in which hydrogen is displaced from the ruthenium and binds to one of the hydrides ($\mathbf{TS_{S5,6}}$). The barrier of this reaction step is 9.5 kcal mol^{-1} and the displacement of dihydrogen is accompanied by a rearrangement of the ruthenium complex from an octahedral to a trigonal-bipyramidal structure. From the product of this step, $\mathbf{6_S}$, the H_2 molecule can dissociate to regenerate $[Ru(CH_3O)H_2\{P(CH_3)_3\}_2]^-$ ($\mathbf{2_S}$; Figure 1), which completes the cycle for pathway **A**. The exergonicity of this last step ($\Delta G = -9.3\ \mathrm{kcal\,mol^{-1}}$) is in large part due to the entropy effect on dissociative processes at high temperature ($-T\Delta S = -15\ \mathrm{kcal\,mol^{-1}}$). Because the process is endothermic ($\Delta H > 0$) by 5.7 kcal mol^{-1}, a small free-energy barrier might exist for the breaking of the hydride–H_2 hydrogen bond of $\mathbf{6_S}$. A barrier in the dissociation enthalpy was searched for but a transition state could not be located. Even if a transition state for this process exists, it will be impossible to find by using the employed methodology. The free-energy barrier for these dissociative processes is determined by the balancing of the enthalpy cost (ΔH) and the entropy gain ($-T\Delta S$) that occur during the lengthening of the distance between the two dissociating species. Therefore the transition states of such processes need to be located on the free-energy surface and not on the potential energy surface as is normally the case in these types of calculations. In this particular case, we do not expect a high free-energy barrier for dissociation. The H_2 molecule in $\mathbf{6_S}$ is bound to the catalyst through a hydrogen bond and these bonds are known to be highly fluxional even at room temperature. Therefore, this final dissociation step should be orders of magnitude faster than the preceding step in which a ruthenium–H_2 bond is broken.

Next, the possibility of an intermolecular proton transfer step was investigated in which the catalyst is protonated by the methanol solvent without coordination of the resulting methoxide ion (pathway **B**). Although direct protonation of one of the hydride moieties of the saturated complex $[RuH_3(H_2C{=}O)\{P(CH_3)_3\}_2]^-$ ($\mathbf{3_S}$) is possible, we found that it is energetically less favorable than the loss of formaldehyde from $\mathbf{3_S}$ and protonation of the resulting unsaturated complex $[RuH_3\{P(CH_3)_3\}_2]^-$ ($\mathbf{4_S}$). Protonation can occur either at the ruthenium center or at one of the hydride ligands, and

this yields either the formal ruthenium(IV) complex $[RuH_4\{P(CH_3)_3\}_2]$ or the ruthenium(II) complex $[RuH_2(H_2)\{P(CH_3)_3\}_2]$ ($\mathbf{7_S}$). The tetrahydride complex is 1.9 kcal mol^{-1} more stable than the ruthenium(II) structure, but the barrier for the interconversion of these two species is very low (4.9 kcal mol^{-1} for the formation of the dihydrogen complex $\mathbf{7_S}$ from the tetrahydride complex). Therefore, it is relatively unimportant in this case which of these two species is formed initially because the formation of dihydrogen in this pathway at least requires the formation of dihydrogen complex $\mathbf{7_S}$.

The formation of $\mathbf{7_S}$ from complex $\mathbf{4_S}$ was found to be highly endergonic ($\Delta G = 21.9$ kcal mol^{-1}) and the protonation step proceeds without an energy barrier. It could be argued that a barrier might exist in solution, but that would most likely be very low from the product side because the product is much higher in energy than the reactant and because there are no bulky ligands to shield the complex from protonation. The dissociation of formaldehyde from $\mathbf{3_S}$ and the subsequent protonation has a combined free-energy cost of 25.4 kcal mol^{-1}. The free-energy change for the subsequent dissociation of the H_2 molecule from $\mathbf{7_S}$ is very small ($\Delta G = -1$ kcal mol^{-1}). This dissociation generates $[RuH_2\{P(CH_3)_3\}_2]$ ($\mathbf{8_S}$ in Figure 1). The possibility that the highly unsaturated 14-electron species $\mathbf{8_S}$ is stabilized by either a formaldehyde or phosphine ligand was investigated, but this proved unfavorable due to the large entropy gain for dissociative processes at 423 K and the strong donating nature of the remaining four ligands in $\mathbf{8_S}$. In contrast to pathway **A**, no transition state for the dissociation process could be located, probably because there is no reorganization at the metal center during this process. In addition, no stable structure could be located in which the released dihydrogen moiety is hydrogen-bonded to one of the hydrides of $\mathbf{8_S}$. A Mulliken population analysis revealed that the negatively charged complex $\mathbf{6_S}$ in pathway **A** induces an electric dipole moment in the H_2 molecule (which has partial charges $+0.12$ and -0.12 on the two hydrogen atoms). The positive end of the H_2 molecule is directed towards the negatively charged ruthenium (-0.88) and one of the hydrides (the hydrogen–hydride distance is 2.97 Å). When the methoxide ion is removed from $\mathbf{6_S}$, generating a structure similar to $\mathbf{8_S}$, the charge on ruthenium decreases (-0.62) and the dipole moment in the H_2 molecule is much smaller (the partial charges decrease to $+0.03$ and -0.03, respectively). As a consequence, a weakly bonded minimum, such as found in pathway **A**, is not stable when the methoxide anion is removed from complex $\mathbf{6_S}$.

In the final step of pathway **B**, the previously generated methoxide ion coordinates to the catalyst to regenerate pentacoordinated complex $\mathbf{2_S}$. Owing to the highly unsaturated nature of $\mathbf{8_S}$, this step is exergonic by 9.3 kcal mol^{-1} in spite of the large entropy penalty for associative processes at high temperature.

A base-dependent dehydrogenation pathway that does not involve initial phosphine dissociation was also investigated (pathway **C**). Although a concerted β-hydride transfer and release of formaldehyde from $\mathbf{1_S}$ would be exergonic by -11 kcal mol^{-1} ($\mathbf{1_S} \rightarrow \mathbf{9_S}$), no transition state could be located for such a process. Note that this transition state would be highly unusual as the complex would effectively be heptacoordinated. Nevertheless, it is possible that β-hydride transfer and the formation of a H_2 ligand occurs in a concerted fashion, circumventing the formation of a real heptacoordinated structure. The potential energy surface in the region in which one would expect such an unusual transition state was scanned carefully to locate a first-order saddle point, but all attempts failed. The optimization either led back to the reactant $\mathbf{1_S}$ or it led to a transition state for β-hydride transfer in which one of the phosphine ligands had dissociated from the complex (i.e., $\mathbf{TS_{S2,3}}$ of pathway **A**). To estimate how high the relative energy of a hypothetical transition state for β-hydride transfer in a complex with three phosphine ligands would be, constrained optimizations were performed by using the distances of the reaction coordinates from the corresponding transition state in the complex with only two phosphine ligands ($\mathbf{TS_{S2,3}}$, Figure 2). To optimize a structure in which all three phosphine moieties are coordinated to the metal, it was necessary to keep all Ru–P distances fixed at the distances in reactant $\mathbf{1_S}$. This investigation revealed that, even if there was a first-order saddle point in a region that could be referred to as a transition state for concerted β-hydride transfer and formaldehyde release, the energy barrier for this process would be very high ($\Delta G >$ 60 kcal mol^{-1}).[29]

Even if β-hydride transfer is not possible for the coordinatively saturated octahedral complex $\mathbf{1_S}$, the resulting trihydride intermediate $\mathbf{9_S}$ could be formed through a crossover from one of the other pathways. This would still allow the remainder of the reaction to proceed through tris-phosphine structures. A connection exists between $[Ru(CH_2{=}O)H_3\{P(CH_3)_3\}_2]^-$ ($\mathbf{3_S}$) in pathways **A** and **B** and $[RuH_3\{P(CH_3)_3\}_3]^-$ ($\mathbf{9_S}$) in pathway **C** through the exchange of formaldehyde for a phosphine ligand. This substitution is endergonic by only 4.1 kcal mol^{-1} (indicated by the line between $\mathbf{3_S}$ and $\mathbf{9_S}$ via $\mathbf{4_S}$ in Figure 1).

As in pathway **B**, proton transfer from methanol to one of the hydrides of the anionic ruthenium trihydride $[RuH_3\{P(CH_3)_3\}_3]^-$ ($\mathbf{9_S}$) was predicted to be highly endergonic (18.3 kcal mol^{-1}) and occurs without a barrier in the gas phase. The dehydrogenation process by this pathway then proceeds with the loss of H_2 from $\mathbf{10_S}$, which generates dihydride complex $\mathbf{11_S}$. In sharp contrast to the hydrogen dissociation in pathway **B**, this process was endergonic ($\Delta G =$ 4.9 kcal mol^{-1}). The entropy gain upon hydrogen dissociation is similar in all three pathways, which indicates that the dihydrogen ligand is bound significantly more strongly to intermediate $\mathbf{10_S}$ than to $\mathbf{7_S}$ in pathway **B**. We attribute this to the influence of the ligand *trans* to the dihydrogen moiety, which is a strongly *trans*-labilizing hydride ligand in $\mathbf{7_S}$ and a much weaker phosphine ligand in $\mathbf{10_S}$.

As we observed in pathway **B**, the reorganization of the dihydrogen ligand from the ruthenium center to one of the hydride ligands in complex $\mathbf{11_S}$ did not lead to a stable hy-

drogen-bonded complex. As discussed above, this seems to be an effect of the total charge of the complex and the magnitude of the induced dipole moment in the dihydrogen molecule. A transition state for direct dissociation of dihydrogen from $\mathbf{10_S}$ was searched for, but could not be located. Performing a constrained optimization, keeping the ruthenium–dihydrogen distance at 3.4 Å, followed by relaxation, led back to complex $\mathbf{10_S}$ without an energy barrier. To close the catalytic cycle of this pathway, the coordinatively unsaturated complex $\mathbf{11_S}$ must react with the previously generated methoxide ion, leading to the formation of complex $\mathbf{1_S}$. Although coordination of a methoxide to the highly unsaturated complex $\mathbf{8_S}$ in pathway **B** is highly exergonic, the same process is less favorable for pentacoordinated intermediate $\mathbf{11_S}$ in this pathway.

By comparison, it is clear that all three pathways studied are predicted to have similar free-energy profiles. From complex $\mathbf{1_S}$, all three proceed through the same initial steps: Phosphine dissociation, β-hydride elimination, and release of formaldehyde. High free-energy barriers for each pathway are found after these initial steps. Figure 1 suggests that the reaction proceeds by an intermolecular protonation of the catalyst followed by release of dihydrogen (pathway **B**). The calculated free-energy barrier, starting from aldehyde complex $\mathbf{3_S}$, is lowest for this pathway ($\Delta G^{\ddagger} = 25.4$ kcal mol^{-1}) and second lowest for pathway **C** ($\Delta G^{\ddagger} = 27.3$ kcal mol^{-1}). Relative to the measured turnover frequency of 6 h^{-1}, which corresponds to an activation free energy of 30 kcal mol^{-1} at 423 K, these two calculated barriers are too low.[10] This could indicate that the reaction is faster when catalyzed by a ruthenium complex containing trimethylphosphine ligands instead of triphenylphosphine ligands. On the other hand, as was discussed previously, there is also an uncertainty in the energetics of CH_3O^- solvation, which leads to an uncertainty in the energetics of protonation steps $\mathbf{4_S} \rightarrow \mathbf{7_S}$ and $\mathbf{9_S} \rightarrow \mathbf{10_S}$ in pathways **B** and **C** and therefore in the predicted overall barriers for these pathways. Because the uncertainty in these pathways is identical, their energy profiles can be compared directly, but they cannot be compared accurately to pathway **A**, which does not involve the solvation of a methoxide species. On the basis of these calculations on a model system we can therefore conclude that pathway **C** is less favorable than pathway **B** but that it is difficult to determine whether pathway **A** or **B** is the lowest-energy pathway.

The effect of dispersion interactions on the thermodynamics of ligand dissociation: Although the free-energy diagrams obtained for the $P(CH_3)_3$-ligated model are in fair agreement with the experimental data, the $P(CH_3)_3$ ligand differs both electronically and sterically from the PPh_3 ligand used in the experimental studies.[25,30] There could be quantitative differences between the calculated free-energy profiles of the model and the full catalyst. Because the energy differences between the three pathways are small, these could alter the preferred reaction pathway. Therefore the lowest-energy pathways investigated above were re-evaluated for the full catalyst. Before discussing these results, however, a particular issue concerning ligand dissociation needs to be addressed.

To our surprise we found that initial phosphine dissociation from starting complex $[Ru(MeO)H_2(PR_3)_3]^-$ ($\mathbf{1_B}$) was predicted to be much more exergonic for PPh_3 in the full catalyst (−38.1 kcal mol^{-1}) than for $P(CH_3)_3$ in the model (−13 kcal mol^{-1}). In addition, the value for the full catalyst is much more exergonic than would be expected based on the experimentally determined free energy for PPh_3 dissociation from a related Ru^{II} compound. For $[Ru(CO)Cl(CH{=}CHPh)(PPh_3)_3]$, a free energy of ligand dissociation of −7 kcal mol^{-1} was measured at 423 K.[31] Because phosphine dissociation plays a key role in discriminating between the different pathways in this study, a further analysis of this discrepancy was required.

To understand the underlying reason for this deviation it was useful to partition the calculated Gibbs free energies of dissociation into enthalpy and entropy terms. As expected, the entropy effect ($-T\Delta S$) for ligand dissociation is very large at this temperature (−25.4 kcal mol^{-1}). This value can be compared with the experimentally determined entropy change of 57.5 ± 7.6 cal mol^{-1} K^{-1} for phosphine dissociation from $[Ru(CO)Cl(CH{=}CHPh)(PPh_3)_3]$.[31] Considering the experimental standard deviation, this value corresponds to a $-T\Delta S$ term of between −21 and −27 kcal mol^{-1} at 423 K. It can thus be concluded that although the computed value of $-T\Delta S$ is large, it reproduces the experimental value rather well.

The agreement between experimental and calculated entropies suggests that the major part of the error in the calculated free energy for phosphine dissociation is in the enthalpy term of the free energy. Sieffert and Bühl recently reported that the B3LYP approach underestimates the gas-phase electronic energy of ligand dissociation from $[Ru(CO)Cl(CH{=}CHPh)(PPh_3)_3]$ by almost 40 kcal mol^{-1} relative to the experimental data.[25] The main reason for the large deviation between the B3LYP and experimental data is the inability of this functional to describe dispersion interactions. Sieffert and Bühl furthermore reported that the dispersion-corrected B3LYP-D and M06 functionals predict values that are in good agreement with experimental data (deviations of 4 and 6 kcal mol^{-1}, respectively, for B3LYP-D and M06). For $[Ru(MeO)H_2(PPh_3)_3]^-$ ($\mathbf{1_B}$), the electronic gas-phase energy for phosphine dissociation predicted by the B3LYP functional in this study is 5.4 kcal mol^{-1}, whereas the corresponding value predicted by the B3LYP-D functional is 37.6 kcal mol^{-1}. The only difference between the B3LYP and the B3LYP-D functionals is the incorporation of an empirical dispersion correction in the latter and the large differences in the energies predicted by these two functionals must therefore be attributed to dispersion interactions. In other words, there is an attractive dispersion force of 32.2 kcal mol^{-1} keeping the PPh_3 ligand bound to the starting complex $\mathbf{1_B}$. The electronic dissociation energy predicted by the M06 functional, which does not contain an empirical dispersion correction term but has instead been parame-

trized to include dispersion forces, is 39.4 kcal mol^{-1}, very similar to the one predicted by the B3LYP-D functional.

To calculate the Gibbs free energy for the dissociation of PPh_3 from $[Ru(MeO)H_2(PPh_3)_3]^-$, the gas-phase electronic energies were corrected for basis-set superposition errors ($\Delta E_{BSSE} = -5.2$ kcal mol^{-1}, determined by using the B3LYP functional and the LACV3P** basis set), dielectric solvent effects ($\Delta E_{SCRF} = -10.7$ kcal mol^{-1}), zero-point vibrational effects, and thermal corrections to the enthalpy ($\Delta H_{CORR} = -2.2$ kcal mol^{-1}) and entropy ($-T\Delta S = -25.4$ kcal mol^{-1}). When these contributions were summed up, B3LYP predicted a Gibbs free energy of dissociation of -38.1 kcal mol^{-1}, whereas B3LYP-D and M06 predicted values of -5.9 and -9.5 kcal mol^{-1}, respectively. To our knowledge there is no experimentally determined equilibrium constant for this particular ligand dissociation process that we could use to validate our computed values, but in light of the reported value for the dissociation of PPh_3 from $[Ru(CO)Cl(CH{=}CHPh)(PPh_3)_3]$ and the corresponding theoretical results, it is reasonable to assume that the dissociation process studied here, as well as other reaction steps in the three pathways that involve dissociation or addition of species to the catalyst, are better described by the B3LYP-D and M06 functionals.

Pathways for the full system (PPh_3 ligands): Both the classical B3LYP and the two dispersion-corrected density functionals were used to construct the free-energy diagram for the full catalyst system (Figure 3). Because B3LYP is known to give good structural properties,[32] the dispersion-corrected functionals were used for single-point energy calculations on B3LYP-optimized structures. Re-optimization of the structures of these large complexes is computationally expensive and is expected to give minor structural changes.[25] In the following we will discuss the free-energy diagrams of both the B3LYP and the B3LYP-D functionals together to show the effects of dispersion forces on the respective pathways. In all cases the B3LYP-D and M06 calculations were found to give very similar results. Therefore the M06 free-energy profile will not be discussed separately, but is given in the Supporting Information (see SI-2 in the Supporting Information).

As for the model system ($P(CH_3)_3$ ligands), the product of phosphine dissociation, $\mathbf{2_B}$, undergoes facile β-hydride elimination to form formaldehyde complex $\mathbf{3_B}$. For the full catalyst system the barrier for this process is 6.4 kcal mol^{-1} (B3LYP), 3.7 kcal mol^{-1} lower than the corresponding barrier for the $P(CH_3)_3$ system. Also, the product is considerably more stable for the full catalyst system than for the $P(CH_3)_3$ system. Because this step does not involve dissociation/coordination of species from/to the catalyst, the effect of including dispersion interactions is smaller than on the previous step. The transition state $\mathbf{TS_{B2,3}}$ is stabilized by 2.2 kcal mol^{-1} and the product $\mathbf{3_B}$ is stabilized by 3.0 kcal mol^{-1} relative to reactant $\mathbf{2_B}$ (B3LYP-D). We attribute this to the reorganization of the structure from a pentacoordinated trigonal-bipyramidal to a hexacoordinated octahedral structure in this reaction and the side-on coordination of the formaldehyde ligand in the product relative to the end-on coordination of the methoxide moiety in the reactant. Due to these features, the product is more sterically crowded than the reactant, which results in more and stronger dispersion interactions within the complex.

In pathway **A**, B3LYP predicted similar free-energy costs for the $P(CH_3)_3$-ligated model and the full PPh_3-ligated system for the loss of formaldehyde from **3** (3.5 and 4.8 kcal mol^{-1}, respectively). As expected, dispersion interactions had a pronounced effect on the thermodynamics of this dissociation step. For the full system, they added an additional free-energy cost of 5.8 kcal mol^{-1}. On the other hand, dispersion forces stabilized the product of the subsequent reaction of $\mathbf{4_B}$ with methanol. Whereas B3LYP predicted similar energy barriers of 27.6 and 28.1 kcal mol^{-1} for the model and the full system, respectively, the dispersion-corrected functional B3LYP-D predicted a barrier of only 18.1 kcal mol^{-1}. When we combined the energy cost of formaldehyde dissociation ($\mathbf{3_B} \rightarrow \mathbf{4_B}$) and this barrier of methanol coordination and proton transfer, the dispersion effects of the two steps largely canceled. B3LYP and B3LYP-D then predicted barriers of 32.9 and 28.7 kcal mol^{-1}, respectively, for this two-step process. This shows that although the dispersion contribution to individual metal–ligand bonds can be large, they can partly cancel if the exchange of two ligands of similar size and polarizability is studied.

From the product $\mathbf{5_B}$, the energy barriers for the reorganization of the dihydrogen molecule from the ruthenium center to one of the hydride moieties predicted by B3LYP for the model system and by B3LYP-D for the full system are almost identical. B3LYP predicted a lower barrier for the full system because it underestimated the strength of the ruthenium–dihydrogen bond in compound $\mathbf{5_B}$ by not taking dispersion interactions into account. Because the dihydrogen molecule is only bound to the product of this step ($\mathbf{6_B}$) through a hydrogen bond, dispersion interactions are not expected to play an important role in determining the strength of the hydride–dihydrogen bond. As a consequence, B3LYP predicted that $\mathbf{5_B}$ is less stable than the product $\mathbf{6_B}$ of this reaction step, whereas the B3LYP-D functional predicted the opposite due to the stabilizing effect of dispersion interactions on reactant $\mathbf{5_B}$. Another consequence is that the effect of dispersion interactions on the final liberation of H_2 from this complex is smaller than one would expect based on the other dissociative processes reported here.

For pathway **B**, the energetics of the intermolecular protonation of $[RuH_3(PR_3)_2]^-$ is strongly dependent on the model and the functional used. B3LYP predicted that this step is endergonic by 21.9 and 17.8 kcal mol^{-1} for the $P(CH_3)_3$ model and the full catalyst, respectively. This contradicts the classic notion that $P(CH_3)_3$ is more electron-donating than PPh_3 and should therefore yield a higher electron density at the metal center and a more basic catalyst.[30] One explanation is that the negative charge in reactant **4** is more shielded from the solvent in bulky complex $\mathbf{4_B}$ than that in model complex $\mathbf{4_S}$, and that this destabilizes **4** relative to neutral product **7**. Note that although this step is neither a dissocia-

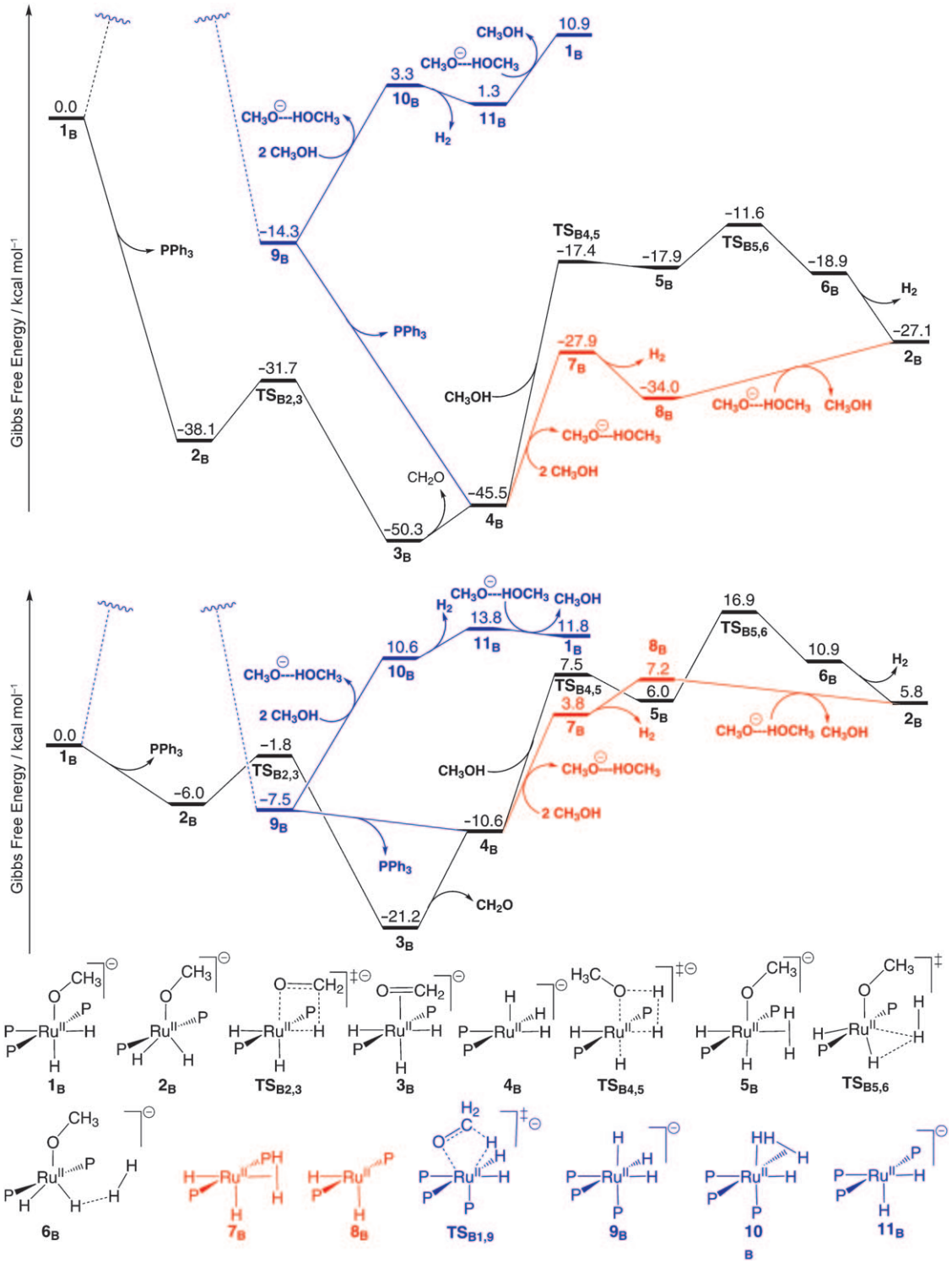

Figure 3. Free-energy profiles for pathways **A**, **B**, and **C** for the full catalyst system, predicted by the B3LYP (top) and B3LYP-D (bottom) functionals. Free energies are reported relative to the starting complex $\mathbf{1_B}$ in kcal mol^{-1}. P represents the PPh_3 ligand.

tive nor an associative process, the inclusion of dispersion interactions does stabilize product $\mathbf{7_B}$ relative to reactant $\mathbf{4_B}$ by 3.4 kcal mol^{-1}.

B3LYP also predicted that the subsequent release of dihydrogen from **7** is more exergonic for the full system than for the model, which suggests that the steric bulk of the PPh_3 ligands enhanced hydrogen dissociation from this complex. The incorporation of dispersion interactions added a considerable attractive force of 9.5 kcal mol^{-1} between the catalyst and the dihydrogen molecule in $\mathbf{7_B}$, thereby stabilizing $\mathbf{7_B}$ relative to product $\mathbf{8_B}$ and making this step endergonic. For the model system we showed that direct β-hydride elimina-

tion from the starting complex $\mathbf{1_S}$ through heptacoordinated transition state $\mathbf{TS_{S1,9}}$ in pathway **C** is inaccessible. For the sterically more hindered full system, such a heptacoordinated transition state is even less likely. Therefore it is reasonable to assume that, as in the model system, trihydride complex $\mathbf{9_B}$ is formed from $\mathbf{1_B}$ in the initial steps of pathways **A** and **B** (i.e., phosphine dissociation, β-hydride elimination, and formaldehyde release) followed by the re-coordination of the phosphine ligand to $[RuH_3(PPh_3)_2]^-$ ($\mathbf{4_B}$). As discussed in the previous section, B3LYP overestimated the free-energy cost for the coordination of a phosphine ligand to intermediate $\mathbf{4_B}$ in the full system by 28.1 kcal mol^{-1}. As a consequence, species $\mathbf{9_B}$ and all subsequent intermediates in pathway **C** were predicted to be high in energy relative to the structures in the other two pathways. When dispersion forces were taken into account using the B3LYP-D functional, however, this reaction step became much less endergonic and this made pathway **C** competitive with the other two pathways.

The free energy of protonation of intermediate $[RuH_3(PR_3)_3]^-$ (**9**) by the solvent is independent of the applied model and functional. Both for the model and the full system, the employed functionals gave values of 17.6–18.3 kcal mol^{-1}. The protonation of **9** leads to only minor structural changes in the catalyst and this results in similar dispersive forces in the reactant **9** and product **10**. The subsequent release of dihydrogen, on the other hand, is a dissociative process and so dispersion interactions play an important role in this step. B3LYP predicted that hydrogen dissociation through this pathway for the full model is exergonic ($\Delta G = 2.0$ kcal mol^{-1}). When dispersion interactions are included, however, reactant $\mathbf{10_B}$ is stabilized by 5.2 kcal mol^{-1} relative to product $\mathbf{11_B}$ and the step becomes endergonic. As in the model system, both a transition state for hydrogen release from $\mathbf{10_B}$ and an intermediate in which the dihydrogen molecule is hydrogen-bonded to one of the hydride moieties of $\mathbf{11_B}$ were searched for, but neither could be located. In the final step of this pathway, a methoxide moiety coordinates to the catalyst. As expected for an associative process, B3LYP strongly underestimated the stability of the product for the full system. B3LYP-D predicted that this step is almost isoenergetic, as B3LYP predicted for the model system.

In summary, the inability of the B3LYP functional to describe dispersion interactions has substantial effects on the free-energy profiles of the pathways described herein. Not only are dissociation energies systematically overestimated and association energies underestimated, the energetics of other steps also deviate by as much as 4 kcal mol^{-1}. Curiously, the free-energy diagram of the model system, in which dispersion interactions play only a minor role, and that of the full catalyst system determined by the B3LYP-D functional are very similar. This indicates that although $P(CH_3)_3$ and PPh_3 are very different ligands, the simple $P(CH_3)_3$ model does reproduce the free-energy diagram of the full system qualitatively. This is important as simplified/reduced models have often been applied to describe complex systems.[27] In the final section we will discuss the catalytic cycle and quantitatively analyze the different pathways for the full catalyst system.

The catalytic cycle of the dehydrogenation reaction: A common feature of the free-energy diagrams determined by all methods and for all the models used in this investigation is that the lowest-energy intermediate was predicted to be the anionic complex $[Ru(CH_2{=}O)H_3(PR_3)_2]^-$ ($\mathbf{3_S}$ and $\mathbf{3_B}$; Figure 1 and Figure 3). From this resting state of the catalyst, it is possible to compare the free-energy profiles of the different pathways and so determine which pathway(s) is/are dominant in the process. The free-energy profiles of the catalytic cycles for the full model (PPh_3) were determined by using the B3LYP-D functional and were used to construct these energy profiles because dispersion-corrected DFT is expected to yield the best quantitative description of the system. The free-energy profiles of the catalytic cycles of the three pathways are shown in Figure 4.

All the pathways show an initial high free-energy cost for the liberation of formaldehyde and subsequent creation of a dihydrogen ligand followed by one or several less energy-demanding steps to form $[RuH_2(CH_3O)(PPh_3)_2]^-$ ($\mathbf{2_B}$). Even the free-energy barrier for the subsequent β-hydride transfer from $\mathbf{2_B}$ is only 4.1 kcal mol^{-1}. For pathway **A**, the total free-energy barrier for the loss of formaldehyde from $\mathbf{3_B}$, methanol coordination, and proton transfer is 28.7 kcal mol^{-1}. From the resulting high-energy polyhydride species $\mathbf{5_B}$, the barrier for hydrogen dissociation is only 10.9 kcal mol^{-1}, but the overall barrier relative to the resting state $\mathbf{3_B}$ is 38.1 kcal mol^{-1}. The transition state for this step, $\mathbf{TS_{B5,6}}$, is 6.9 kcal mol^{-1} higher in energy than the transition state for the final β-hydride elimination step, $\mathbf{TS_{B2,3}}$, which indicates that hydrogen dissociation is the rate-determining step in this pathway. The calculated overall barrier for dehydrogenation by pathway **A** is too high, however, for this pathway to be of significance at the experimental reaction temperature of 423 K.

Despite the low barrier for the β-hydride transfer step from $\mathbf{2_B}$, its transition state, $\mathbf{TS_{B2,3}}$, is the highest point in the free-energy profile of pathway **B**. Thus, although a large part of the overall barrier of dehydrogenation is caused by the formation of high-energy intermediate $[RuH_2(CH_3O)(PPh_3)_2]^-$ ($\mathbf{2_B}$) from the resting state $\mathbf{3_B}$, the subsequent β-hydride transfer was predicted to be the rate-determining step in the catalytic cycle by this pathway. The computed overall activation free energy for the dehydrogenation of methanol ($\mathbf{3_B} \rightarrow \mathbf{TS_{B2,3}}$) by pathway **B** is 31.2 kcal mol^{-1}, which is in good agreement with the experimentally reported rate of 6 h^{-1} ($\Delta G^{\neq} = 30$ kcal mol^{-1}).[10]

As discussed previously, this absolute value suffers from a larger uncertainty due to issues in describing the solvation of the small methoxide anion. Because the solvation of the methoxide anion is described in the same way in pathways **B** and **C**, it is possible to directly compare the free-energy profiles of these two pathways. From Figure 4 it is clear that pathway **B** is favored over pathway **C**. Tris-phosphine inter-

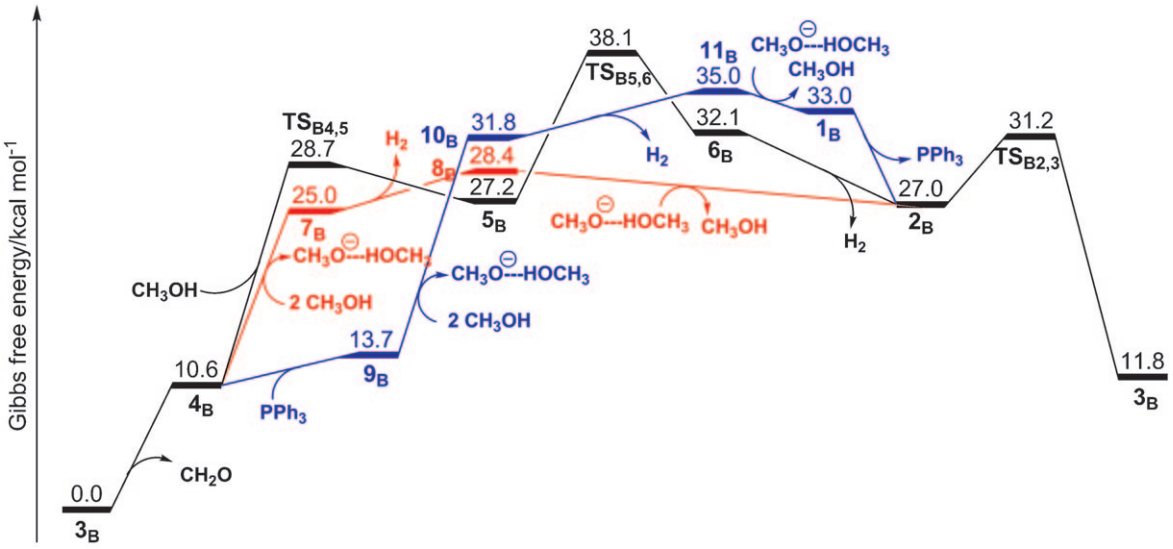

Figure 4. Free-energy profiles for pathways **A** (black), **B** (red), and **C** (blue) for the full catalyst system, predicted by the B3LYP-D functional. Free energies are reported relative to the resting state $\mathbf{3_B}$ in kcal mol^{-1}.

mediates $\mathbf{11_B}$ and $\mathbf{1_B}$ in pathway **C** are both higher in energy than their bis-phosphine analogues $\mathbf{8_B}$ and $\mathbf{2_B}$, in spite of the strongly attractive dispersion interactions that exist between the PPh_3 ligands and the metal complexes in this study. This is attributable to the large negative entropy change that occurs upon coordination of a phosphine ligand to complex $\mathbf{4_B}$ at the high reaction temperature used for this process. Our calculations therefore reproduce the results from previous kinetic studies that showed that the reaction rate is inversely proportional to the ligand concentration.[12] They predict that, under the experimental conditions, the reaction preferentially proceeds via complexes that contain only two phosphine ligands. From the calculated free-energy profiles we can deduce that higher ligand concentrations would shift the ligand dissociation equilibria $\mathbf{4_B}\rightarrow\mathbf{9_B}$ and $\mathbf{2_B}\rightarrow\mathbf{1_B}$ (Figure 3) towards the coordinatively saturated complexes $[RuH_2(CH_3O)(PPh_3)_3]^-$ ($\mathbf{9_B}$) and $[RuH_3(PPh_3)_3]^-$ ($\mathbf{1_B}$). This will inhibit both the protonation of $\mathbf{4_B}$ and β-hydride elimination from $\mathbf{2_B}$ and therefore slow down the dehydrogenation process.

A final note on the accuracy of the free energies presented herein can be made by comparing the computed free energy for the overall reaction to experimental data. The predicted reaction free energy for the catalytic conversion of methanol to formaldehyde and hydrogen gas is determined by the energy difference between two consecutive occurrences of the resting state $\mathbf{3_B}$ in the free-energy profile (Figure 3). The calculated reaction enthalpies (ΔH) and free energies (ΔG) are compared with experimental data in Table 1. For all three density functionals (B3LYP, B3LYP-D, and M06) the predicted enthalpy and free energy deviate by less than 2.7 kcal mol^{-1} from the experimental values.

Table 1. Computed and experimental thermodynamic parameters for the process $CH_3OH\rightarrow CH_2{=}O+H_2$ at room temperature and 423 K.[a]

Method	$T=298$ K		$T=423$ K	
	ΔH	ΔG	ΔH	ΔG
B3LYP	22.4	14.5	22.9	11
B3LYP-D	23.2	15.3	23.7	11.8
M06	24.8	16.9	25.3	13.4
exp.[b]	22.1	14.3	–	11

[a] Values of ΔH and ΔG are given in units of kcal mol^{-1}. [b] See ref. [33].

Conclusion

DFT and transition-state theory (TST) have been used to investigate the possible reaction pathways for the dehydrogenation of methanol in the presence of $[Ru(OCH_3)H_2(PPh_3)_3]^-$ ($\mathbf{1_B}$) as catalyst under basic conditions. Three density functionals were used; the classical B3LYP functional and the dispersion-corrected functionals B3LYP-D and M06. We have shown that dispersion interactions play a crucial role in ligand dissociation/association processes. For the dissociation of a PPh_3 ligand, the observed dispersion effect is especially large (around 30 kcal mol^{-1}), but also for other reaction steps studied herein dispersion effects are non-negligible for accurate prediction of reaction kinetics.

For the dehydrogenation of methanol, our calculations suggest that the resting state of the catalyst is the trihydride complex $[RuH_3(CH_2{=}O)(PR_3)_2]^-$ ($\mathbf{3_S}$ or $\mathbf{3_B}$). This species can liberate formaldehyde and then be protonated by a methanol molecule. All models and density functionals applied in this investigation predict the same mechanism, that is, an intermolecular proton transfer followed by hydrogen release and coordination of a methoxide anion and finally β-hydride transfer to regenerate the resting state. From our calcula-

tions it is difficult to assign the rate-determining step with certainty because multiple steps in the process are found to have very similar barriers. However, the calculations show that a large part of the overall free-energy barrier is caused by the initial steps in the catalytic cycle, that is, the dissociation of formaldehyde from the resting state of the catalyst and protonation of the resulting species by the alcoholic solvent. The predicted overall activation energy of the process was found to be between 29.6 and 31.4 kcal mol^{-1} (depending on the density functional applied), which is in good agreement with the experimentally observed reaction rate.[34]

Acknowledgements

This research was supported by the Fonds der Chemischen Industrie and by the Cluster of Excellence (Tailor-Made Fuels from Biomass) funded by the Excellence Initiative of the German federal and state governments. The Rechen- und Kommunikationszentrum at RWTH Aachen University is acknowledged for the use of its computational facilities. We also thank Professor D. J. Cole-Hamilton for stimulating comments on the manuscript.

[1] For selected examples of the use of hydrogen in the production of fuels from biomass, see: a) A. Corma, S. Iborra, A. Velty, *Chem. Rev.* **2007**, *107*, 2411–2502; b) G. W. Huber, A. Corma, *Angew. Chem.* **2007**, *119*, 7320–7338; *Angew. Chem. Int. Ed.* **2007**, *46*, 7184–7201; c) J. N. Chheda, G. W. Huber, J. A. Dumesic, *Angew. Chem.* **2007**, *119*, 7298–7318; *Angew. Chem. Int. Ed.* **2007**, *46*, 7164–7183; d) Y. Román-Leshkov, C. J. Barrett, Z. Y. Liu, J. A. Dumesic, *Nature* **2007**, *447*, 982–986.

[2] For recent examples of important publications in this field, see: a) S. W. Kohl, L. Weiner, L. Schwartsburd, L. Konstantinovski, L. J. Shimon, Y. Ben-David, M. A. Iron, D. Milstein, *Science* **2009**, *324*, 74–77; b) D. G. Nocera, *Inorg. Chem.* **2009**, *48*, 10001–10017; c) J. L. Dempsey, B. S. Brunschwig, J. R. Winkler, H. B. Gray, *Acc. Chem. Res.* **2009**, *42*, 1995–2004; d) M. W. Kanan, D. G. Nocera, *Science* **2008**, *321*, 1072–1075; e) K. Maeda, K. Teramura, D. Lu, T. Takata, N. Saito, Y. Inoue, K. Domen, *Nature* **2006**, *440*, 295; f) F. Gärtner, B. Sundararaju, A.-E. Surkus, A. Boddien, B. Loges, H. Junge, P. H. Dixneuf, M. Beller, *Angew. Chem.* **2009**, *121*, 10147–10150; *Angew. Chem. Int. Ed.* **2009**, *48*, 9962–9965; g) A. Kudo, Y. Miseki, *Chem. Soc. Rev.* **2009**, *38*, 253–278; h) N. D. McDaniel, F. J. Coughlin, L. L. Tinker, S. Bernhard, *J. Am. Chem. Soc.* **2008**, *130*, 210–217; i) J. F. Hull, D. Balcells, J. D. Blakemore, C. D. Incarvito, O. Eisenstein, G. W. Brudvig, R. H. Crabtree, *J. Am. Chem. Soc.* **2009**, *131*, 8730–8731; j) H. Kunkely, A. Vogler, *Angew. Chem.* **2009**, *121*, 1713–1715; *Angew. Chem. Int. Ed.* **2009**, *48*, 1685–1687; k) J. J. Concepcion, J. W. Jurss, M. K. Brennaman, P. G. Hoertz, A. O. T. Patrocinio, N. Y. M. Iha, J. L. Templeton, T. J. Meyer, *Acc. Chem. Res.* **2009**, *42*, 1954–1965.

[3] R. M. Navarro, M. C. Sánchez-Sánchez, M. C. Alvarez-Galvan, F. del Valle, J. L. G. Fierro, *Energy Environ. Sci.* **2009**, *2*, 35–54.

[4] a) T. A. Milne, C. C. Elam, R. J. Evans, *Hydrogen From Biomass, State of the Art and Challenges*, **2002**, IEA/H2/TR-02/001; b) G. Van Rossum, B. Potic, S. R. A. Kersten, W. P. M. Van Swaaij, *Catal. Today* **2009**, *145*, 10–18; c) M. Ni, D. Y. C. Leung, M. K. H. Leung, K. Sumathy, *Fuel Process. Technol.* **2006**, *87*, 461–472.

[5] B. Kamm, P. R. Gruber, M. Kamm, *Biorefineries—Industrial Processes and Products*, Wiley-VCH, Weinheim, **2006**.

[6] For a recent review, see: A. Friedrich, S. Schneider, *ChemCatChem* **2009**, *1*, 72–73.

[7] For selected examples, see: a) R. D. Cortright, R. R. Davda, J. A. Dumesic, *Nature* **2002**, *418*, 964–967; b) H. Jacobsen, *Angew. Chem.* **2004**, *116*, 1948–1950; *Angew. Chem. Int. Ed.* **2004**, *43*, 1912–1914; c) G. W. Huber, J. W. Shabaker, J. A. Dumesic, *Science* **2003**, *300*, 2075–2077.

[8] A. Dobsen, S. D. Robinson, *J. Organomet. Chem.* **1975**, *87*, C52–C53.

[9] a) G. R. A. Adair, J. M. J. Williams, *Tetrahedron Lett.* **2005**, *46*, 8233–8235; b) G. B. W. L. Ligthart, R. H. Meijer, M. P. J. Donners, J. Meuldijk, J. A. J. M. Vekemans, L. A. Hulshof, *Tetrahedron Lett.* **2003**, *44*, 1507–1509; c) A. Dobson, S. D. Robinson, *Inorg. Chem.* **1977**, *16*, 137–142; d) C. W. Jung, P. E. Garrou, *Organometallics* **1982**, *1*, 658–666; e) S. Shinoda, H. Itagaki, Y. Saito, *J. Chem. Soc. Chem. Commun.* **1985**, 860–861; f) J. van Buijtenen, J. Meuldijk, J. A. J. M. Vekemans, L. A. Hulshof, H. Kooijman, A. L. Spek, *Organometallics* **2006**, *25*, 873–881.

[10] a) D. Morton, D. J. Cole-Hamilton, *J. Chem. Soc. Chem. Commun.* **1988**, 1154–1156; b) D. Morton, D. J. Cole-Hamilton, I. D. Utuk, M. Paneque-Sosa, M. Lopez-Poveda, *J. Chem. Soc. Dalton Trans.* **1989**, 489–495.

[11] a) J. Halpern, *J. Organomet. Chem.* **1987**, *330*, 155–159; b) D. R. Linn, Jr., J. Halpern, *J. Am. Chem. Soc.* **1987**, *109*, 2969–2974.

[12] L.-C. Yang, T. Ishida, T. Yamakawa, S. Shinoda, *J. Mol. Catal. A* **1996**, *108*, 87–93.

[13] a) H. Junge, M. Beller, *Tetrahedron Lett.* **2005**, *46*, 1031–1034; b) H. Junge, A. Boddien, F. Capitta, B. Loges, J. R. Noyes, S. Gladiali, M. Beller, *Tetrahedron Lett.* **2009**, *50*, 1603–1606; c) B. Loges, A. Boddien, H. Junge, J. R. Noyes, W. Baumann, M. Beller, *Chem. Commun.* **2009**, 4185–4187.

[14] H. Junge, B. Loges, M. Beller, *Chem. Commun.* **2007**, 522–524.

[15] a) J. Zhang, M. Gandelman, L. J. W. Shimon, H. Rozenberg, D. Milstein, *Organometallics* **2004**, *23*, 4026–4033; b) J. Zhang, G. Leitus, Y. Ben-David, D. Milstein, *J. Am. Chem. Soc.* **2005**, *127*, 10840–10841; c) J. Yhao, J. F. Hartwig, *Organometallics* **2005**, *24*, 2441–2446; d) C. P. Casey, J. B. Johnson, S. W. Singer, Q. Cui, *J. Am. Chem. Soc.* **2005**, *127*, 3100–3109; e) C. Gunanathan, Y. Ben-David, D. Milstein, *Science* **2007**, *317*, 790–792; f) J. Zhang, M. Gandelman, L. J. W. Shimon, D. Milstein, *J. Chem. Soc. Dalton Trans.* **2007**, 107–113; g) K.-I. Fujita, N. Tanino, R. Yamaguchi, *Org. Lett.* **2007**, *9*, 109–111.

[16] a) A. D. Becke, *J. Chem. Phys.* **1993**, *98*, 5648–5652; b) C. Lee, W. Yang, R. G. Parr, *Phys. Rev. B* **1988**, *37*, 785–789; c) S. H. Vosko, L. Wilk, M. Nusair, *Can. J. Phys.* **1980**, *58*, 1200–1211; d) P. J. Stephens, F. J. Devlin, C. F. Chabalowski, M. J. Frisch, *J. Phys. Chem.* **1994**, *98*, 11623–11627.

[17] Jaguar 7.0, Schrödinger LLC, Portland, New York NY, **2007**.

[18] P. J. Hay, W. R. Wadt, *J. Chem. Phys.* **1985**, *82*, 299–310.

[19] Y. Zhao, D. G. Truhlar, *Acc. Chem. Res.* **2008**, *41*, 157–167.

[20] S. Grimme, *J. Comput. Chem.* **2006**, *27*, 1787–1799.

[21] TURBOMOLE V6.0, **2009**, University of Karlsruhe and Forschungszentrum Karlsruhe GmbH, **1989–2007**, TURBOMOLE GmbH, since **2007**, available from http://www.turbomole.com.

[22] Gaussian 03, revision C.02, M. J. Frisch, G. W. Trucks, H. B. Schlegel, G. E. Scuseria, M. A. Robb, J. R. Cheeseman, J. A. Montgomery, Jr., T. Vreven, K. N. Kudin, J. C. Burant, J. M. Millam, S. S. Iyengar, J. Tomasi, V. Barone, B. Mennucci, M. Cossi, G. Scalmani, N. Rega, G. A. Petersson, H. Nakatsuji, M. Hada, M. Ehara, K. Toyota, R. Fukuda, J. Hasegawa, M. Ishida, T. Nakajima, Y. Honda, O. Kitao, H. Nakai, M. Klene, X. Li, J. E. Knox, H. P. Hratchian, J. B. Cross, V. Bakken, C. Adamo, J. Jaramillo, R. Gomperts, R. E. Stratmann, O. Yazyev, A. J. Austin, R. Cammi, C. Pomelli, J. W. Ochterski, P. Y. Ayala, K. Morokuma, G. A. Voth, P. Salvador, J. J. Dannenberg, V. G. Zakrzewski, S. Dapprich, A. D. Daniels, M. C. Strain, O. Farkas, D. K. Malick, A. D. Rabuck, K. Raghavachari, J. B. Foresman, J. V. Ortiz, Q. Cui, A. G. Baboul, S. Clifford, J. Cioslowski, B. B. Stefanov, G. Liu, A. Liashenko, P. Piskorz, I. Komaromi, R. L. Martin, D. J. Fox, T. Keith, M. A. Al-Laham, C. Y. Peng, A. Nanayakkara, M. Challacombe, P. M. W. Gill, B. Johnson, W. Chen, M. W. Wong, C. Gonzalez, J. A. Pople, Gaussian, Inc., Wallingford CT, **2004**.

[23] J. W. Ochterski, *Thermochemistry in Gaussian*, Gaussian Inc., Wallingford **2000**.
[24] F. B. van Duijneveldt, J. G. C. M. van Duijneveldt-van de Rijdt, J. H. van Lenthe, *Chem. Rev.* **1994**, *94*, 1873–1885.
[25] N. Sieffert, M. Bühl, *Inorg. Chem.* **2009**, *48*, 4622–4624.
[26] D. J. Tannor, B. Marten, R. Murphy, R. A. Friesner, D. Sitkoff, A. Nicholls, B. Honig, M. Ringnalda, W. A. Goddard III, *J. Am. Chem. Soc.* **1994**, *116*, 11875–11882.
[27] P. E. M. Siegbahn, *J. Comput. Chem.* **2001**, *22*, 1634–1645.
[28] M. Ahlquist, S. Kozuch, S. Shaik, D. Tanner, P. O. Norrby, *Organometallics* **2006**, *25*, 45–47.
[29] This transition state was searched for starting from both the *fac* and *mer* isomers of complex $\mathbf{1_S}$.
[30] C. A. Tolman, *J. Am. Chem. Soc.* **1970**, *92*, 2953–2956.
[31] S. K. Seetharaman, M.-C. Chung, U. Englich, K. Ruhlandt-Senge, M. B. Sponsler, *Inorg. Chem.* **2007**, *46*, 561–567.
[32] a) M. R. A. Blomberg, P. E. M. Siegbahn, M. Svensson, *J. Chem. Phys.* **1996**, *104*, 9546–9554; b) A. Ricca, C. W. Bauschlicher, *J. Phys. Chem. A* **1997**, *101*, 8949–8955; c) A. Ricca, C. W. Bauschlicher, *J. Phys. Chem. A* **1994**, *98*, 12899–12903.
[33] *Standard Thermodynamic Properties of Chemical Substances in CRC Handbook of Chemistry and Physics, Internet Version 2005* (Ed.: D. R. Lide), CRC Press, Boca Raton, **2005**.
[34] During the revision of the manuscript related findings have been reported, see: N. Sieffert, M. Bühl, *J. Am. Chem. Soc.* **2010**, *132*, 8056–8070.

Received: March 6, 2010
Published online: October 7, 2010

